Available online at www.sciencedirect.com
ScienceDirect
Journal of Sound and Vibration 307 (2007) 662–679
JOURNAL OF SOUND AND VIBRATION
www.elsevier.com/locate/jsvi

Interactions between nonlinear spur gear dynamics and surface wear

Huali Ding, Ahmet Kahraman*

Department of Mechanical Engineering, The Ohio State University, 201 West 19th Avenue, Columbus, OH 43210, USA

Received 17 November 2005; received in revised form 11 October 2006; accepted 26 June 2007
Available online 21 August 2007

Abstract

In this study, two different dynamic models, a finite elements-based deformable-body model and a simplified discrete model, and a surface wear model are combined to study the interaction between gear surface wear and gear dynamic response. The proposed dynamic gear wear model includes the influence of worn surface profiles on dynamic tooth forces and transmission error as well as the influence of dynamic tooth forces on wear profiles. This paper first introduces the nonlinear dynamic models that include gear backlash and time-varying gear mesh stiffness, and a wear model separately. It presents a comparison to experiments for validation of the dynamic models. The dynamic models are combined with the wear model to study the interaction of surface wear and dynamic behavior in both linear and nonlinear response regimes. At the end, several sets of simulation results are used to demonstrate the two-way relationship between nonlinear gear dynamics and surface wear.

1. Introduction

Dynamic behavior of gear systems has attracted many investigators for two primary reasons. One reason is the fatigue life of the gear pair. Dynamic gear tooth forces are typically larger than the corresponding quasi-static forces, resulting in larger dynamic stresses and shorter bending and contact fatigue lives. The second primary reason for dynamic modeling is gear noise. Time-varying dynamic gear mesh and bearing forces are transmitted to surrounding structures through the housing and the mounts to cause gear whine noise. Therefore, large vibration amplitudes typically result in higher noise levels as well.

While gear durability and noise are the most obvious concerns requiring a better understanding of dynamic behavior of a gear train, there are a host of other failure modes or functional behavior that are influenced by gear dynamics as well. Among them, surface wear of gears seems to be the most interesting and challenging one, since the influences are in both directions. The dynamic behavior of the gears amounts to tooth forces that are different from the quasi-static forces in both magnitude and shape. These tooth forces also reflect various nonlinear phenomena such as backlash-induced tooth separations, jump discontinuities, and sub-harmonic parametric resonances. Therefore, surface wear outcome is strongly related to the contact stresses

*Corresponding author. Tel.: +1 614 292 4678; fax: +1 614 292 3163.
E-mail address: kahraman.1@osu.edu (A. Kahraman).

0022-460X/$ - see front matter © 2007 Elsevier Ltd. All rights reserved.
doi:10.1016/j.jsv.2007.06.030

and the dynamic behavior. In addition, like the dynamic response amplitudes, wear behavior should also vary with speed as well. On the other hand, dynamic response of a gear pair is very sensitive to deviations of the tooth surface profiles from a perfect involute. Intentional tooth modifications such as tip and root relieves are commonly used to reduce the dynamic forces at a certain design torque. Unavoidable manufacturing errors also influence the dynamic response since they act as a "transmission error" excitation at the gear mesh interface. Surface wear is a material removal process that results in a deviation from the intended tooth profiles. Therefore, a gear pair with worn surfaces should have dynamic behavior that is quite different from a gear pair with no wear. This indicates that gear dynamics and gear wear are mutually dependent on each other.

In this study, this apparent link between the dynamic behavior of a spur gear pair and tooth surface wear will be studied. Dynamic models of varying complexity and a quasi-static wear model will be proposed. A dynamic wear prediction methodology will be developed to describe the impact of dynamics on surface wear as well as the impact of wear on gear pair dynamics.

1.1. Literature survey

A large number of published theoretical and experimental spur gear dynamics studies focused on either noise or durability. Most of these studies proposed discrete models to predict the parameters that might be related to the gear noise levels (e.g. Refs. [1–4]). In line with the experimental studies on spur gear dynamics [4–8], these nonlinear time-varying models used discrete gear mesh interface formulations that include periodic mesh stiffness and gear backlash-induced tooth separations. In addition, an external displacement excitation was included in some of these models to represent gear profile errors and intentional tooth modifications. Both the mesh stiffness function and the displacement excitation would be determined by using a static-elastic gear contact (load distribution) model. One commonly used output from these models was the dynamic transmission error (DTE) that is defined as

$$\mathrm{DTE} = r_p\theta_p(t) + r_g\theta_g(t). \tag{1}$$

It represents the motion transmission error along the line of action of gears where r_p and r_g are the base radii of gears 1 and 2, and θ_p and θ_g are the angular displacements. This is the dynamic equivalent of the better-known static transmission error (STE).

Tooth bending and contact fatigue-related failure modes of spur gear pairs can be improved through better design practices, materials, and lubricants. Gears that are optimized for these failure modes often exhibit surface wear since they operate longer life cycles. Besides the direct material loss that leads to functional failure and potentially higher gear noise levels, surface wear can also affect the patterns of gear contact. This might alter stresses and load distribution to accelerate the occurrence of other failure modes [9].

Sliding wear of a lubricated surface can be described by the initial value problem [10]

$$\frac{\mathrm{d}h}{\mathrm{d}s} = F(P, u, \ldots), \tag{2}$$

where h is the wear depth, s is the relative sliding distance and F is a function of a number of parameters influencing wear including contact pressure P, sliding velocity u, hardness, surface roughness, and lubricant-related parameters. Wear accumulation can be calculated by integrating Eq. (2), provided that the function F is known. Archard [10] proposed a simple model that takes probability of asperity collision into account in the form of a wear coefficient k. Although more advanced wear models were also proposed using different methodologies and parameter sets, Archard's wear model still remains the most commonly used model for practical applications.

There are a few studies on prediction of spur gear wear under quasi-static conditions. Flodin and Andersson [11] calculated the sliding distance from involute profile geometry. They determined the load carried by each tooth pair in the mesh and calculated contact pressures using a simplified Winkler's mattress model where a surface represented by independent springs carrying the load. The values of contact pressure and sliding distance were then combined in Archard's wear model to determine the wear profile in involute direction. The contact pressure calculations were repeated incrementally to account for the changes in pressure due to wear

of the contacting surfaces. They did not include the influence of intentional tooth surface modifications, tooth profile errors and tooth deflections in their models. They also did not provide any experimental validation. The gear wear model of Bajpai et al. [12] addressed some of these open issues. Their wear prediction methodology included both intentional surface modifications and manufacturing/assembly-related imperfections. They also performed a number of tightly controlled gear wear experiments under quasi-static conditions to validate their wear model. Yuksel and Kahraman [13] applied a similar wear model to a deformable-body dynamic model of a planetary gear set to demonstrate the influence of representative tooth wear profiles on planetary gear set dynamics.

1.2. Objectives and scope

Currently, very little is known of wear behavior of gears under dynamic conditions. The wear models cited above were strictly static as they relied on the load distribution and tooth forces predicted under quasi-static conditions. On the other hand, dynamic models cited were not equipped to consider the influence of a worn gear tooth surface on dynamic response. This paper, therefore, focuses in bridging this gap between the dynamics and wear models. A pair of dynamic models and a static gear wear model developed earlier will be introduced and modified to arrive at a dynamic gear wear model. Technical challenges in achieving this goal will be presented together with potential strategies in eliminating them. Numerical results on an example spur gear pair will be presented to demonstrate wear-dynamics interactions and related future research topics will be outlined.

2. Gear pair dynamic model

In this study, the spur gear dynamic models of Tamminana et al. [14] will be adapted. The first one of these models is a finite elements (FE)-based deformable body model that was developed by using a special-purpose contact analysis software [15]. The model divides the gear into a near-field region near the contact, and a far-field region away from the contact. The FE method is used to compute relative deformations and stresses for points in the far field, and a semi-analytical deformation model based on the Bousinesq and Cerruti solutions is used in the near field within the contact zones. This approach does not require a highly refined mesh at the contacting tooth surfaces, reducing the computational effort compared to conventional FE models which require a refined mesh at the gear tooth region, limiting the model to static analysis only. Therefore, the model used here allows a more refined and comprehensive study of spur gear dynamics using a truly deformable-body formulation. The tooth surfaces are modeled by a large number of nodes representing the involute shape and surface modifications. The model makes it unnecessary to locally refine the FE mesh near the contact, and re-mesh the finite elements for each contact position. A reference frame is attached to the pinion and gear, and the finite element computations are done for each of them separately. The mesh stiffness and mesh contact forces, comprising the dynamic excitation for the system, are evaluated internally at each time step [15]. Contact conditions are handled as linear inequality constraints whose solution is obtained by a revised Simplex solver. Contact analysis determines the contact conditions between the pinion and gear at each time step. Both rigid body motions and the FE displacement vector are considered for each gear to satisfy the linear system of differential equations [15] with Rayleigh's damping model. The deformable-body model employs a time-discretization scheme based on Newmark method. We refer to Tamminana et al. [14] for a detailed description of the application of the contact model to a spur gear pair dynamics problem.

The deformable-body model, while accurate and detailed, is computationally demanding. Since the dynamic wear simulations will require a large number of real-time analyses, the second dynamic model seeks a more computationally efficient alternative to the deformable-body model. This discrete nonlinear, time-varying model shown in Fig. 1 consists of two rigid wheels of polar mass moments of inertia of I_p and I_g, and base radii of r_p and r_g. A periodically time-varying mesh stiffness function $k(t)$ that represents the parametric excitation due to the mesh stiffness variation caused by the fluctuation of number of tooth pairs in contact zone and a viscous damper c connect the two gear wheels along the line of action. A backlash function g is included to represent the gear backlash of magnitude $2b$ and an external displacement excitation $e(t)$ is also applied at the gear mesh interface to represent manufacturing errors, intentional modifications of the tooth profile or a wear

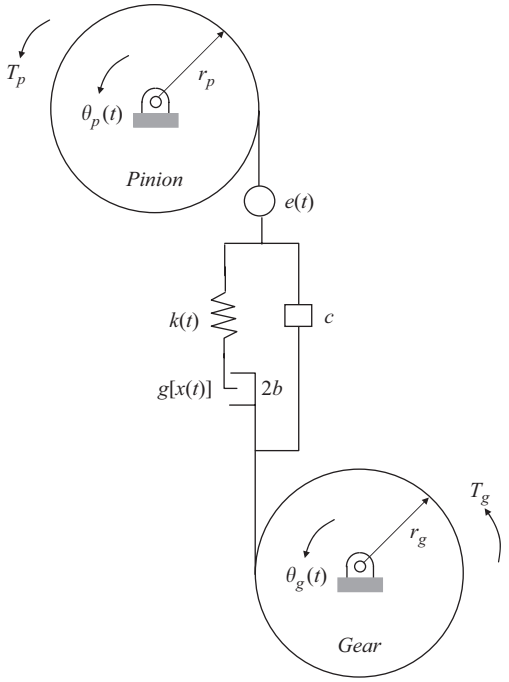

Fig. 1. Discrete dynamic model of a spur gear pair (from Ref. [14]).

profile. Given $F = m_e(T_p r_p/I_p + T_g r_g/I_g)$ and $m_e = I_p I_g/(I_p r_g^2 + I_g r_p^2)$, the governing equation of motion of the single-degree-of-freedom dynamic model is given for a coordinate $x(t) = r_p\theta_p(t) + r_g\theta_g(t) - e(t)$ as [14]

$$m_e\ddot{x} + c\dot{x} + k(t)g[x(t)] = F - m_e\ddot{e}(t), \tag{3a}$$

$$g[x(t)] = \begin{cases} x(t) - b, & x(t) > b, \\ 0, & |x(t)| \leqslant b, \\ x(t) + b, & x(t) < -b, \end{cases} \tag{3b}$$

where an overdot denotes differentiation with respect to time t, and T_p and T_g are constant torque values applied to the pinion and gear, respectively. In the above equations, $x(t)$ represents the difference between DTE and the unloaded STE. This model relies on a gear load distribution model [16] for computations of $k(t)$ and $e(t)$ under quasi-static conditions. This load distribution model is designed to compute elastic deformations of gear tooth surfaces using the tooth compliance and the initial separations under no load. Conditions for compatibility and equilibrium are used to predict the load distribution, tooth forces and $e(t)$. This model computes $k(t)$ and $e(t)$ very fast. The involute profile modifications or wear profiles are represented in the dynamic model by $e(t)$ that corresponds to STE under unloaded conditions. Therefore, a quasi-static load distribution analysis is performed under unloaded conditions for several discrete positions over one mesh cycle to determine $e(t)$. Similarly, the mesh stiffness function $k(t)$ is obtained from the same quasi-static load distribution model, now under operating load conditions. The nonlinear differential equation of motion (3) is solved numerically.

Tamminana et al. [14] compared the predictions of the discrete and deformable-body dynamic models with experiments to demonstrate its accuracy. As an example, Fig. 2 compares root-mean-square (rms) DTE values predicted by the two dynamic models to the measured data for a unity-ratio spur gear pair operated at a 150 mm center distance [4]. Gears forming this pair have 50 teeth, 3 mm module, 20° pressure angle, and an involute contact ratio of ICR = 1.8. Experiment and simulations were performed under both speed-up and speed-down conditions within a range of 500–4000 rpm (gear mesh frequency 415–3330 Hz) so that jump-up

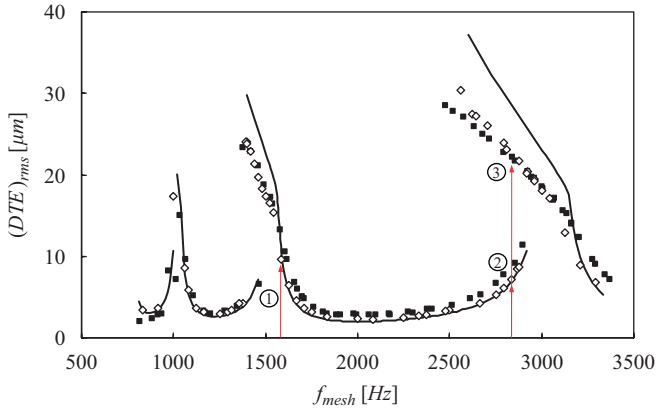

Fig. 2. Comparison of DTE predictions of the dynamic models to measurements at 340 N m (from Ref. [14]). (■) Experiment, (◇) deformable-body model, and (—) discrete model.

and jump-down-type nonlinear phenomena due to tooth separation can be captured. Predictions of the deformable-body model match the measured data very well in terms of both overall amplitudes and the shape of the forced response. The measured primary resonance near 3000 Hz as well as the first two super-harmonic resonances near 1500 and 1000 Hz are predicted accurately by the deformable-body model. The amplitudes of the DTE are also predicted accurately in both resonance and off-resonance regions. In addition, the measured nonlinear behavior characterized by a frequency range of dual stable motions (a lower branch no-contact-loss motion and an upper branch tooth separation motion) bounded by jump-up and jump-down discontinuities also match well with the experimental data. The same conclusions can also be reached for the discrete model with the exception that the DTE predictions of this model along the upper branch tooth separation motions are somewhat larger than the experimental data. This slight discrepancy can be tolerated for many engineering applications since it is much faster. Comparisons to experimental data from other gear pairs having different parameters were also made in Ref. [14] with the same level of agreement to conclude that both models are indeed capable of predicting the dynamic response of a gear pair accurately.

3. Quasi-static gear wear model

The wear model used in this study is based on the model proposed by Bajpai et al. [12] to study the wear of gears under quasi-static conditions. A brief description of the wear model will be offered here as a more detailed presentation of the model and its validation can be found in Ref. [12]. The gear wear model employs Archard's wear equation that can be expressed for a local point on one of the contacting surfaces in relative sliding as

$$h = \int kP\,\mathrm{d}s. \tag{4}$$

Here k is a dimensional wear coefficient, P is the contact pressure amplitude, and s is the sliding distance between this local point and the mating point on the mating gear.

Computation of the wear depth h follows the methodology outlined in Fig. 3. The first step is to determine the initial geometric descriptions of the gear tooth surfaces to serve as the initial state for the wear prediction. The tooth surface modifications must be included in quantifying the initial contact of the gear surfaces. Surface deviations from a perfect involute at a point ij on gears p and g, including surface modifications, are defined as G^p_{ij} and G^g_{ij}, respectively. By selecting points ij at the nodes of a predetermined surface grid, a discretized description of both contacting surfaces are obtained. The second step is the computation of the contact pressure at each nodal point ij at different rotational positions of the gears in mesh. The geometric data consisting of G^ℓ_{ij}, $\ell = p, g$, are input into the same contact mechanics models [15,16] to predict the instantaneous contact pressure distribution $(P^\ell_{ij})_r$ at each rotational position $r \in [0, R]$. Here, the total number of rotational positions R and the increment of the rotation are such that the amount of gear rotation achieved

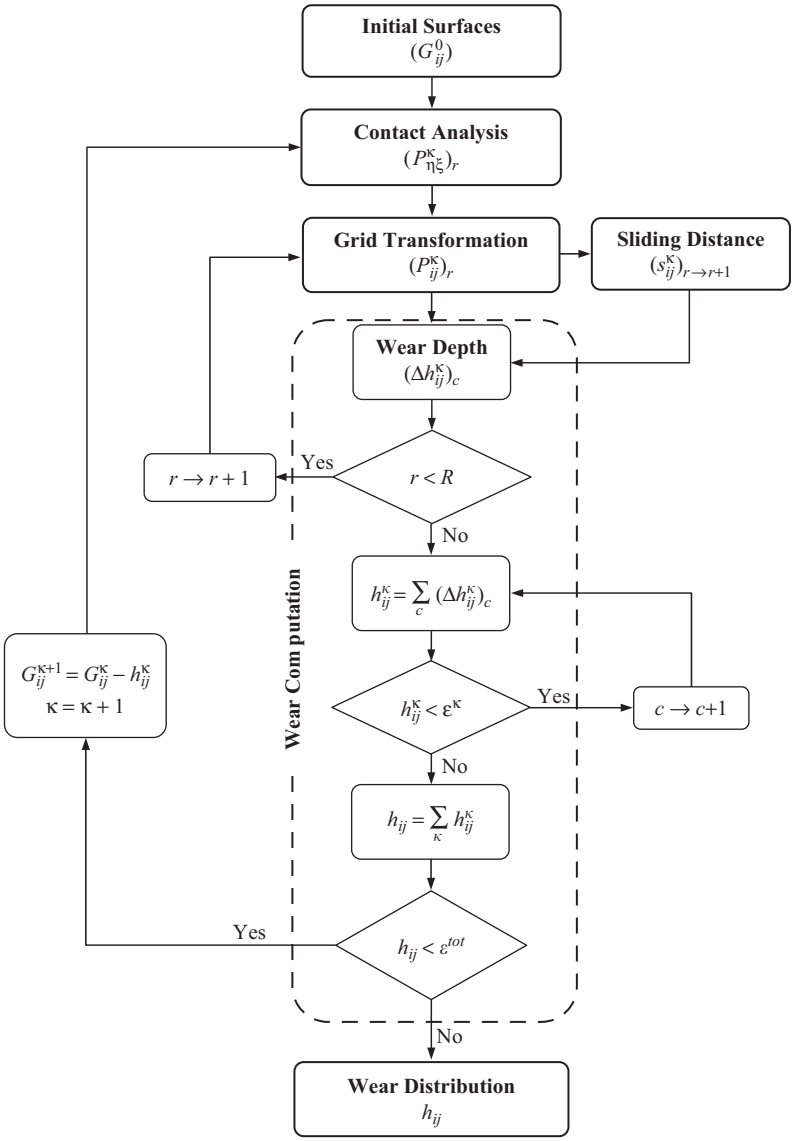

Fig. 3. Methodology used for computation of gear surface wear [12].

covers a complete wear cycle from the position where the tooth of interest enters the mesh zone ($r = 0$) to the position where the tooth exits the mesh zone completely ($r = R$).

Active tooth surfaces of both gears p and g are discretized by $I+1$ equally spaced lead lines along the profile direction and $J+1$ equally spaced profile lines along the lead direction. Hence, the contact pressures at each position r are calculated at the nodes ij of this surface grid on both gears ($i \in [0, I]$ and $j \in [0, J]$) resulting in $(I+1) \times (J+1)$ number of points per tooth to represent the contact surfaces. Considering the ith grid line of the tooth on gear p in the profile direction at a radius R_i^p, the involute angle is $\Phi_i^p = \tan[\cos^{-1}(R_b^p/R_i^p)] - \cos^{-1}(R_b^p/R_i^p)$ where R_b^p is the base circle radius, as illustrated in Fig. 4. At the first rotational position $r = 0$, the position vector of a nodal point at R_i^p and $j = 0$ is defined as

$$(\mathbf{X}_{i0}^p)_{r=0} = \begin{Bmatrix} R_i^p \sin \Phi_i^p \\ R_i^p \cos \Phi_i^p \\ 0 \end{Bmatrix}. \tag{5}$$

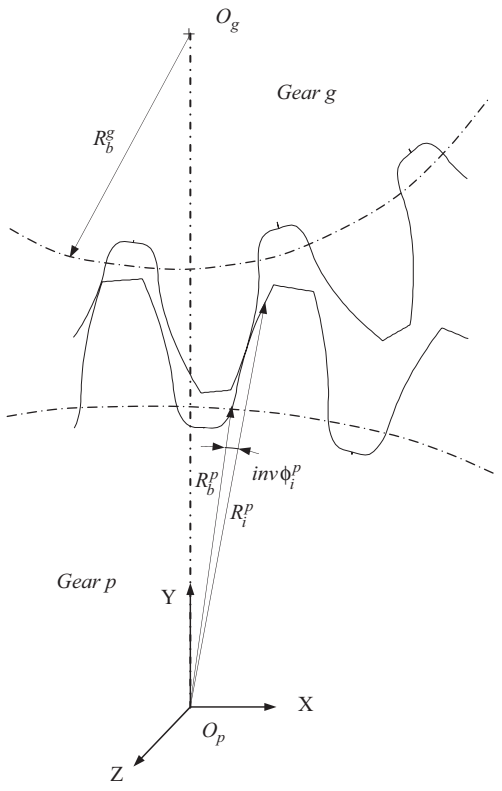

Fig. 4. Basic gear coordinates and the involute angle [12].

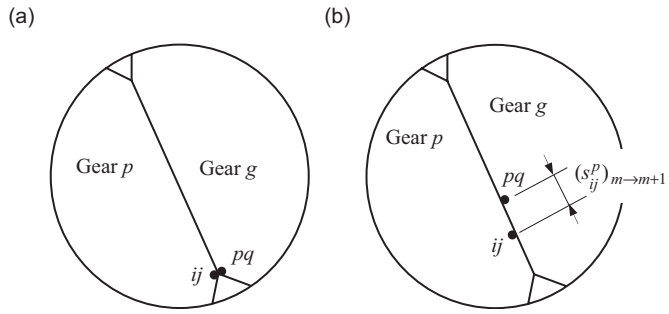

Fig. 5. Illustration of sliding distance of a contact point on the tooth surface at position (a) $r = m$ and (b) $r = m+1$ [12].

At the same radius, the position vector of a node ij at a distance z^p along the gear face from the $j = 0$ edge is given at any position r as

$$(\mathbf{X}_{ij}^p)_r = \mathbf{R}_{r\Delta\theta^p}[\mathbf{R}_{\varphi_{ij}^p}(\mathbf{X}_{ij}^p)_{r=0} + \mathbf{T}_{z^p}]. \tag{6}$$

Here $\varphi_{ij}^p = z^p \tan \psi_i^p / R_i^p$, ψ_i^p is the helix angle at radius R_i^p, $r\Delta\theta^p$ is the angular position of gear p measured from $r = 0$, and $\mathbf{R}$ and $\mathbf{T}$ are the rotation matrix and the translation vector, respectively.

The sliding distance $(s_{ij}^p)_{r\to r+1}$ is defined as the distance by which a point represented by node ij on gear p slides with respect to its corresponding point on its mating gear as they rotate from position r to position $r+1$. As illustrated in Fig. 5(a), when the leading edge of the contact zone reaches a node ij of gear p at $r = m$, node ij meshes with node pq of gear g and experiences a non-zero pressure for the first time since the beginning of

the loading cycle. Position vector $(\mathbf{X}_{ij}^{p})_{r=m}$ of node ij at $r=m$ is given by Eq. (6) and since points ij and pq overlap in space, $(\mathbf{X}_{pq}^{g})_{r=m}=(\mathbf{X}_{ij}^{p})_{r=m}$. When the gears are rotated by one incremental rotation to position to $r=m+1$ as shown in Fig. 5(b), $(\mathbf{X}_{ij}^{p})_{r=m+1}$ is again defined by Eq. (6). Meanwhile, node pq on gear g no longer overlaps with node ij on gear p as gear g rotates about its own center. The position vector of node pq is obtained by first translating the coordinate frame from the center of gear p to the center of gear g, then rotating it by $\Delta\theta^{g}$, and finally translating it back to the center of gear p:

$$(\mathbf{X}_{pq}^{g})_{r=m+1}=\mathbf{R}_{\Delta\theta^{g}}\{(\mathbf{X}_{pq}^{g})_{r=m}+\mathbf{T}_{E}\}-\mathbf{T}_{E}. \tag{7}$$

Here, $\Delta\theta^{g}=-(Z^{p}/Z^{g})\,\Delta\theta^{p}$, Z^{p} and Z^{g} are the number of teeth of gears p and g, respectively, and E is the center distance. If node ij remains within the contact zone until position $r=t$, the sliding distance that occurs when gears rotate from any position r to $r+1$ can be given in general terms as

$$(s_{ij}^{p})_{r\to r+1}=\begin{cases}\left|\left\|(\mathbf{X}_{pq}^{g})_{r+1}-(\mathbf{X}_{ij}^{p})_{r+1}\right\|-\sum_{u=m}^{r}(s_{ij}^{p})_{(u-1)\to u}\right|, & m\leqslant r\leqslant t,\\ 0 & \text{else.}\end{cases} \tag{8}$$

The sliding distance of the corresponding node pq on gear g, $(s_{pq}^{g})_{r\to r+1}$, is also determined by using the same procedure.

Given $(P_{ij}^{\ell})_{r}$ and $(s_{ij}^{\ell})_{r\to r+1}$ $(\ell=p,\,g)$, at every node point ij of both gears, $i\in[0,\,I]$ and $j\in[0,\,J]$, and every rotational position $r\in[0,\,R]$, a discretized version of Eq. (4) can be used to calculate the wear occurred at node ij as gears rotate from position r to $r+1$:

$$(\delta h_{ij}^{\ell})_{r\to r+1}=\tfrac{1}{2}k^{\ell}(s_{ij}^{\ell})_{r\to r+1}[(P_{ij}^{\ell})_{r}+(P_{ij}^{\ell})_{r+1}]. \tag{9}$$

Thus, the total wear depth reached at the same node after one complete wear cycle is

$$\Delta h_{ij}^{\ell}=\sum_{r=0}^{R-1}(\delta h_{ij}^{\ell})_{r\to r+1}. \tag{10}$$

Eqs. (9)–(10) are applied continuously C^{κ} times until the maximum wear depth accumulated at any node of either one of the contacting surfaces after the κth pressure update equals ε^{κ}. Then, the wear amount at nodes ij of gears p and g accumulated after the κth pressure update can be written as

$$(h_{ij}^{\kappa})^{\ell}=\sum_{c=1}^{C^{\kappa}}(\Delta h_{ij}^{\kappa})_{c}^{\ell}. \tag{11}$$

After carrying out the iterations until Kth geometry update ($\kappa=0,\,1,\,2,\ldots,\,K$) when a point on either gear surface reaches the maximum allowable wear value of $\varepsilon^{\mathrm{tot}}$, the cumulative wear depth distribution at node ij just before the Kth update is given by

$$h_{ij}^{\ell}=\sum_{\kappa=1}^{K}(h_{ij}^{\kappa})^{\ell}. \tag{12}$$

Finally, the total number of wear cycles becomes $C^{\mathrm{tot}}=\sum_{\kappa=1}^{K}C^{\kappa}$.

4. Dynamic wear model

With the dynamic gear pair models and the quasi-static wear models available, the next step is to combine them to study the interaction between dynamic response and surface wear. There are three essential additions that must be made for this purpose: (i) the dynamic models must have the capability to consider complex surface deviations due to wear, (ii) the deformable-body contact model that provides tooth forces and contact pressures to the wear model must be a dynamic one, and (iii) the wear model must account for the changes in the wear coefficient due to the changes in lubricant film that is speed dependent. The first two items have been taken care of in the previous sections. The deformable-body dynamic model presented in Section 2 has the ability to include any regular or irregular profile deviations such as a wear profile. The discrete-parameter

dynamic model can do the same since its displacement excitations come from the load distribution model. In addition, as illustrated in Section 3, the deformable-body contact model can simulate the dynamic conditions.

Approximate methods are available for accounting for the influence of lubrication conditions at the gear mesh contact on the wear coefficient k. In most gear applications, geometric, kinematic, lubricant, and surface texture conditions are such that an elastohydrodynamic lubrication (EHL) regime exists. In addition, the fluid film thickness values are comparable to the asperity heights such that actual metal-to-metal contacts are common. In this case, a portion of the contact load is carried by asperities while the rest is supported by the fluid film itself, and the EHL regime is considered as "mixed" or "partial". As the thickness of the fluid film is dependent on speed, one would expect k to change with speed as well. Priest and Taylor [17] proposed an approximate wear coefficient model to account for the effect of film thickness on wear profiles of piston rings. They expressed the wear coefficient k as

$$k = \begin{cases} k_0, & \lambda < \frac{1}{2}, \\ \frac{2}{7}k_0(4-\lambda), & \frac{1}{2} < \lambda < 4, \\ 0, & \lambda > 4. \end{cases} \tag{13}$$

Here, λ is the so-called lambda ratio defined as the ratio of the minimum film thickness $h_{\min}$ to the composite surface roughness $R_q = [R_{qp}^2 + R_{qg}^2]^{1/2}$ where R_{qp} and R_{qg} are the root-mean-square surface

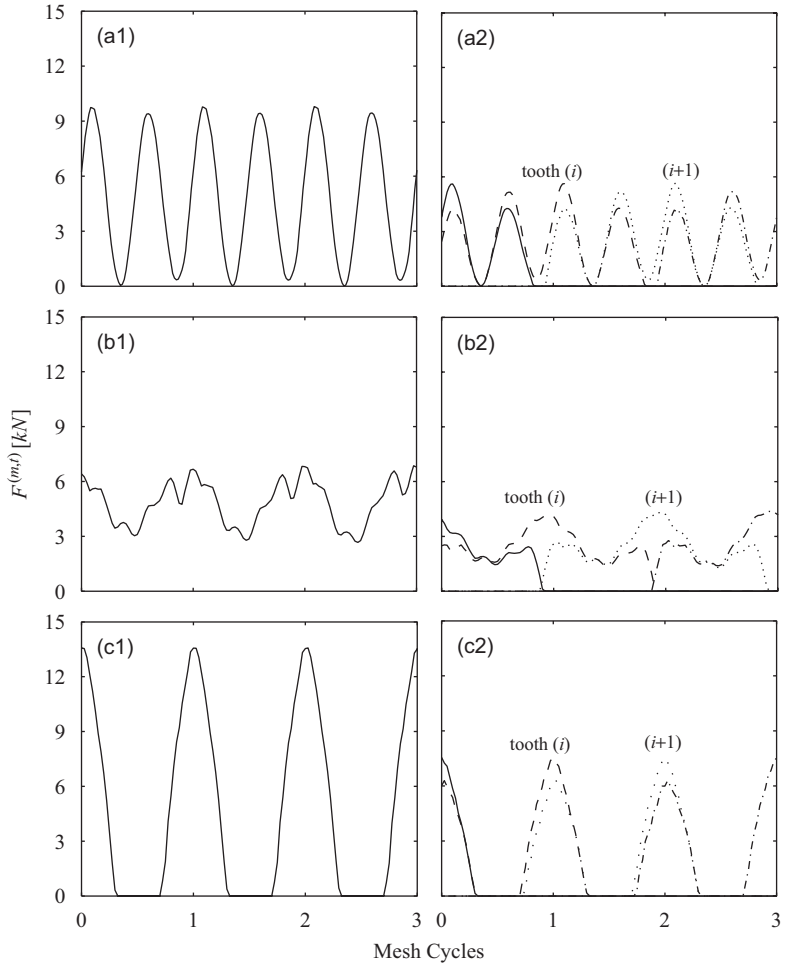

Fig. 6. Time histories of (a1–c1) $F^{(m)}$ and (a2–c2) $F^{(t)}$ of the example gear pair with no wear at (a) 1540 Hz, (b) 2700 Hz on the lower branch, and (c) 2700 Hz on the upper branch.

roughness values of gears p and g at a contact point in the direction of the involute profile. Eq. (13) assumes that the wear coefficient is equal to k_0 for $\lambda<\frac{1}{2}$ that corresponds to the values observed at relatively low speeds such as the ones measured by Bajpai et al. [12]. It also assumes that $k=0$ for $\lambda>4$, i.e. no wear will occur if $h_{\min}$ is at least four times more than R_q. In the transition region within $\frac{1}{2}<\lambda<4$, k reduces linearly from k_0 to zero. Dowson [18] defined $h_{\min}$ of an elliptical contact of two smooth surfaces as

$$\frac{h_{\min}}{R}=3.63U^{0.68}G^{0.49}W^{-0.073}(1-\mathrm{e}^{-0.68\kappa}), \tag{14}$$

where κ is an ellipticity parameter that can be assumed as infinity for any spur gear contact. The dimensionless speed, load and material parameters are defined as $U=\eta_0 u/(E'R)$, $W=(L/b)/(E'R^2)$, and $G=\alpha E'$ where

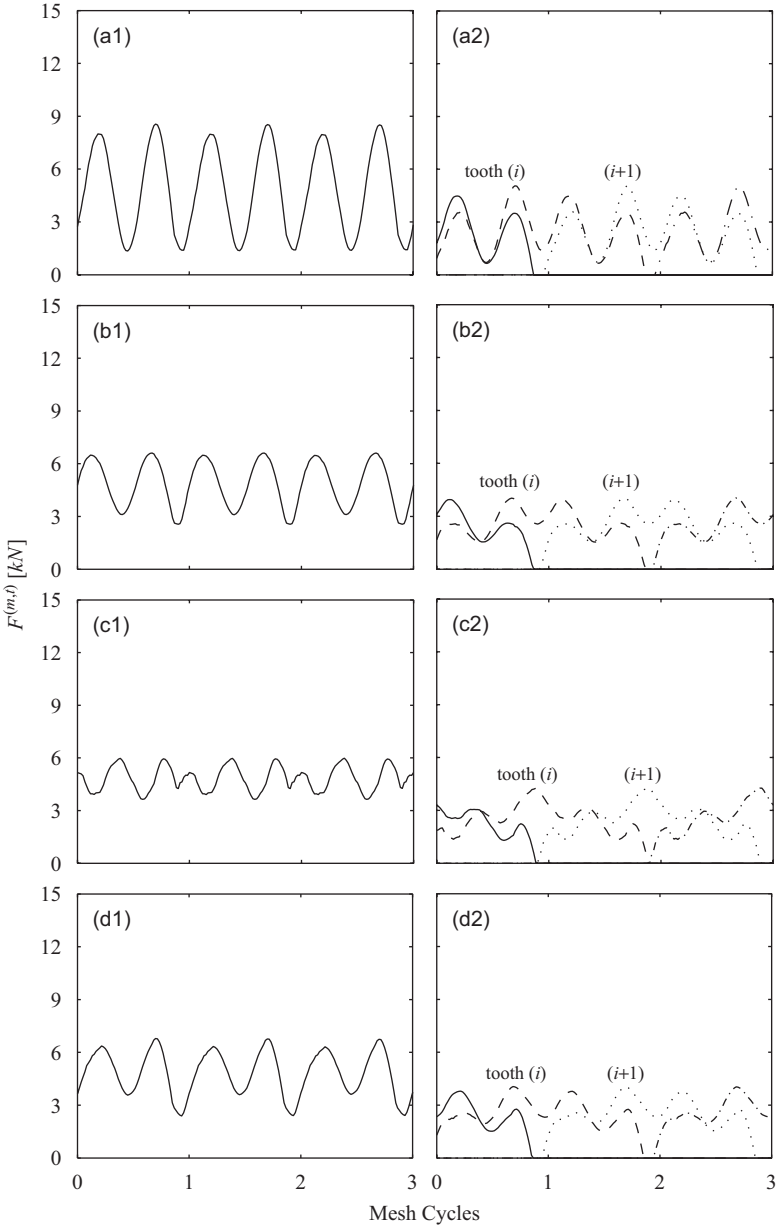

Fig. 7. Time histories of (a1–d1) $F^{(m)}$ and (a2–d2) $F^{(t)}$ of the example gear pair run at 1540 Hz after (a) 2 million cycles, (b) 10 million cycles, (c) 30 million cycles, and (d) 60 million cycles.

L/b is the load per length, u is the average tangential velocity, η_0 is absolute viscosity at reference ambient pressure, and α is the pressure-viscosity coefficient of the lubricant. Here R and E' are the equivalent radius and elasticity of the gear pair defined respectively as

$$\frac{1}{R}=\frac{1}{R_p}+\frac{1}{R_g}, \quad \frac{1}{E'}=\frac{1}{2}\left(\frac{1-v_p^2}{E_p}+\frac{1-v_g^2}{E_g}\right), \tag{15a,b}$$

where R_i is the radius of curvature of gear i, and E_i and v_i are the modulus of elasticity and the Poisson's ratio for the material of gear i. With these relationships, $h_{\min}$ along the gear tooth surfaces are predicted to determine the wear coefficients, which are updated whenever wear threshold value ε^{κ} is reached to update the gear geometry.

After each geometry update, the gear surface with wear is fed into the dynamic models to compute the dynamic contact pressure distribution, which is input to the wear model to predict the wear depth distributions under dynamic conditions as a function of loading cycles. The iterative procedure shown in Fig. 3 is applied until the total cycles of interest or the maximum allowable wear depth value are reached.

5. Results and discussion

In order to demonstrate the dynamic wear model proposed in this study, an example spur gear pair whose dynamic response is shown in Fig. 2 is considered. Wear simulations are performed at three representative operating speeds: (1) at $f_{\text{mesh}}=1540\,\text{Hz}$ (1850 rpm) slightly above the first super-harmonic resonance peak, (2) at $f_{\text{mesh}}=2700\,\text{Hz}$ (3250 rpm) when the gear pair is operated on the lower branch just before the jump-up frequency near the primary resonance peak, and (3) again at $f_{\text{mesh}}=2700\,\text{Hz}$ when the gear pair is operated on the upper branch. These three representative operating conditions are marked in Fig. 2.

A typical automotive transmission fluid operating at $100\,^{\circ}\text{C}$ with $\eta_0=6.5\times10^{-3}\,\text{Pa}^{-1}$, $\alpha=1.2773\times10^{-8}\,\text{Pa}^{-1}$ is used in the simulations. A constant surface roughness value of $R_{qi}=0.2\,\mu\text{m}$ is considered for each gear for the determination of lambda ratio λ. A wear threshold value of $\varepsilon^{\kappa}=1.5\,\mu\text{m}$ for each geometry update is used. As both dynamic models resulted in very similar wear distributions, only the results from the discrete model are shown in the following sections. In these simulations, $k_0=2.5\times10^{-18}\,\text{m}^2/\text{N}$ is used in line with Ref. [12].

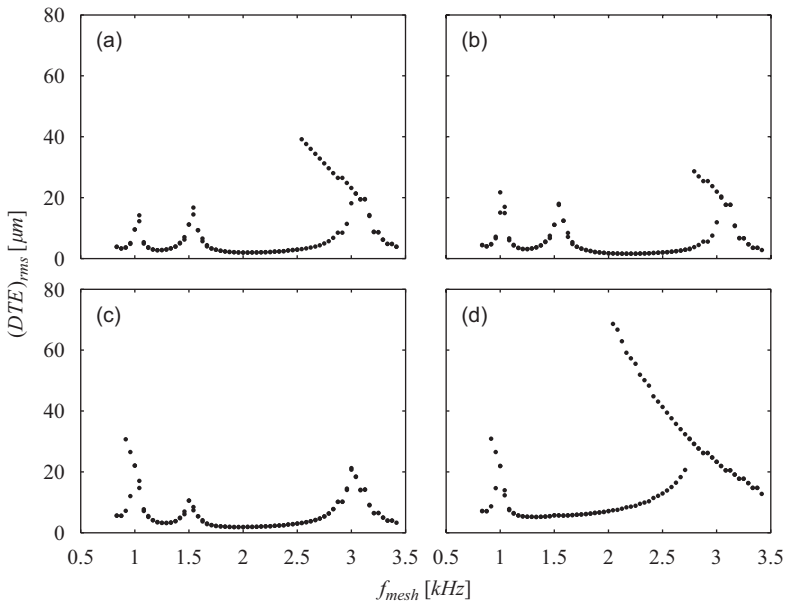

Fig. 8. Forced response of the example gear pair after operation at 1540 Hz for (a) 2 million cycles, (b) 10 million cycles, (c) 30 million cycles, and (d) 60 million cycles.

5.1. Effect of wear on the dynamic response

Before the impact of wear on dynamic behavior can be demonstrated, the dynamic behavior must be established for the baseline case of no surface wear. The predicted total gear mesh force $F^{(m)}$ and individual tooth forces $F^{(t)}$ at the operating conditions marked in Fig. 2 as points 1–3 are shown in Fig. 6 for the gear pair having no wear. Since the involute contact ratio of this example gear pair is 1.8, each tooth pair remains in contact for nearly 1.8 mesh periods, and for nearly 80 percent of the time, there are two tooth pairs in contact. The mesh force $F^{(m)}$ is computed by summing up all of the tooth forces $F^{(t)}$ at any given instant of time. $F^{(m)}$ and $F^{(t)}$ shown Fig. 6(a) at the operating point 1 (1540 Hz) has two cycles per mesh period since the rotational

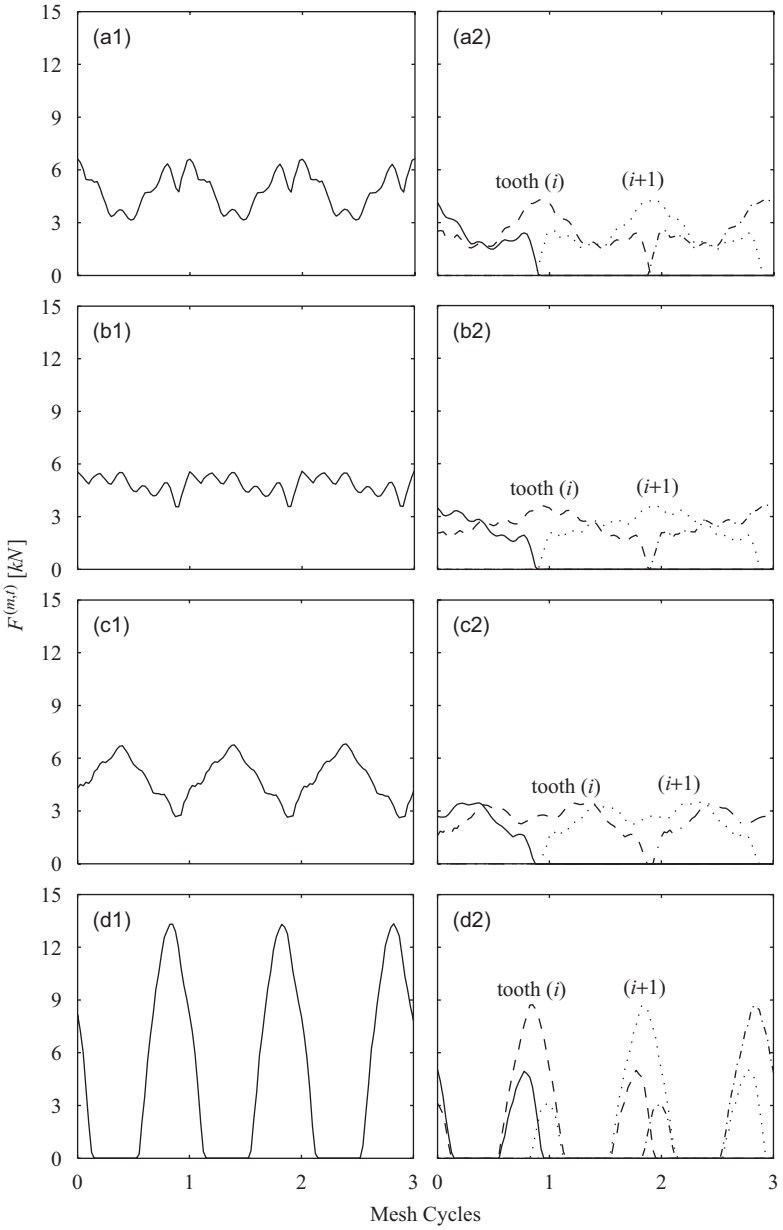

Fig. 9. Time histories of (a1–d1) $F^{(m)}$ and (a2–d2) $F^{(t)}$ of the example gear pair run at 2700 Hz on the lower branch after (a) 2 million cycles, (b) 10 million cycles, (c) 30 million cycles, and (d) 60 million cycles.

speed is near the resonance peak caused by the first harmonic component of the excitations. Here, $F^{(m)}$ becomes almost zero at two positions in each mesh period suggesting that the system is at the threshold of tooth separations. The same is observed in time histories of $F^{(t)}$ as well. Figs. 6(b) and (c) illustrate $F^{(m)}$ and $F^{(t)}$ at the lower and upper branches of the steady-state motions at 2700 Hz (operating points 2 and 3 in Fig. 2), respectively. In Fig. 6(b), $F^{(m)}$ for the lower branch motion always has a non-zero value while $F^{(m)}$ becomes zero for about 40 percent of the time in Fig. 6(c) for the upper branch solution. This is directly due to the nonlinear behavior caused by contact losses (tooth separations).

The influence of wear accumulated at 1540 Hz (operating point 1 in Fig. 2 at 1850 rpm) on the dynamic response is illustrated in Figs. 7 and 8. In Fig. 7, peak-to-peak $F^{(m)}$ amplitudes reduce significantly with wear, reaching their minimum at 30 million cycles, beyond which an increase of $F^{(m)}$ amplitudes is predicted. The steady-state rms DTE amplitudes of the same gear pairs operated at 1850 rpm at different numbers of wear cycles are compared in Fig. 8. It is observed that the amplitude of the first super-harmonic resonance peak at 1500 Hz is reduced significantly with wear cycles before it is fully eliminated with the accumulation of surface wear after 60 million cycles. Very similar to Fig. 6, the gear tooth surfaces wear in a certain shape to eliminate the first harmonic component of the response, resulting in no resonance peak at this speed. While the gears attempt to "correct" themselves at this particular frequency of 1540 Hz, the other resonance peaks are also altered. The second super-harmonic resonance peak is increased significantly due to wear accumulated by operating the gears near the first super-harmonic resonance peak. This peak at 1000 Hz becomes significantly larger in Fig. 8(c–d) with apparent jump discontinuities. Meanwhile, the amplitude of the primary resonance peak at 3000 Hz is also reduced significantly with the wear cycles accumulated at 1540 Hz. After 30 million wear cycles, the resonance peak becomes linear with rather small rms DTE amplitudes. Additional wear cycles beyond this point bring back the jump discontinuities with much larger upper branch DTE amplitudes than those shown in Fig. 2.

The next operating speed of 3250 rpm (2700 Hz) in Fig. 2 is considered to accumulate wear on both lower and upper branches of the steady-state response near the primary resonance peak of the same gear pair. First, the variation of the dynamic forces and the DTE forced response with wear accumulated on the lower branch is presented in Figs. 9 and 10. Here, wear accumulated at this speed on the lower branch after 10 million cycles is sufficient to completely eliminate any tooth separations and softening-type nonlinear behavior observed in Fig. 2 at the primary resonance peak. Peak-to-peak mesh force values reduce drastically after 10 million cycles

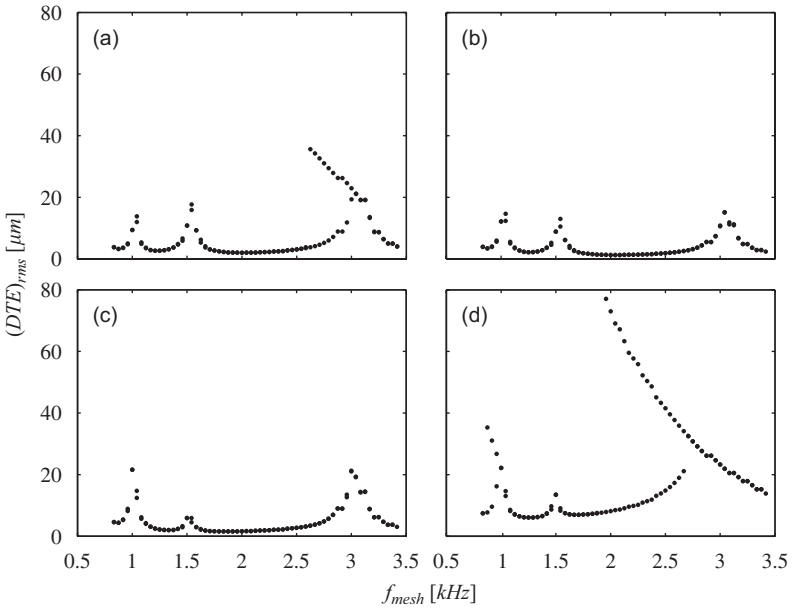

Fig. 10. Forced response of the example gear pair after operation at 2700 Hz on the lower branch for (a) 2 million cycles, (b) 10 million cycles, (c) 30 million cycles, and (d) 60 million cycles.

as well. Additional wear cycles at the same condition increase the nonlinear behavior significantly. There is no lower branch motion at 2700 Hz after 60 million cycles. As a result, the $F^{(m)}$ time history shown in Fig. 9(d) exhibits severe tooth separations during about 40 percent of the mesh cycle. This can be considered as a very significant (both qualitative and quantitative) change induced solely by wear on the dynamic response of the gear pair. The same high level of sensitivity to wear is also obvious in Figs. 11 and 12, which show the influence of the wear accumulation at the upper branch (2700 Hz) on dynamic response. In Fig. 11(a), the tooth separations observed in the $F^{(m)}$ time history shown in Fig. 6(d) for the unworn gear pair are eliminated immediately after only 2 million wear cycles at 2700 Hz on the upper branch. In Fig. 11(b and c), the peak-to-peak $F^{(m)}$ increases steadily with wear cycles and the tooth separations are reintroduced after 60 million wear cycles as shown in Fig. 11(d). The DTE forced responses shown in Fig. 12 at different wear cycles further

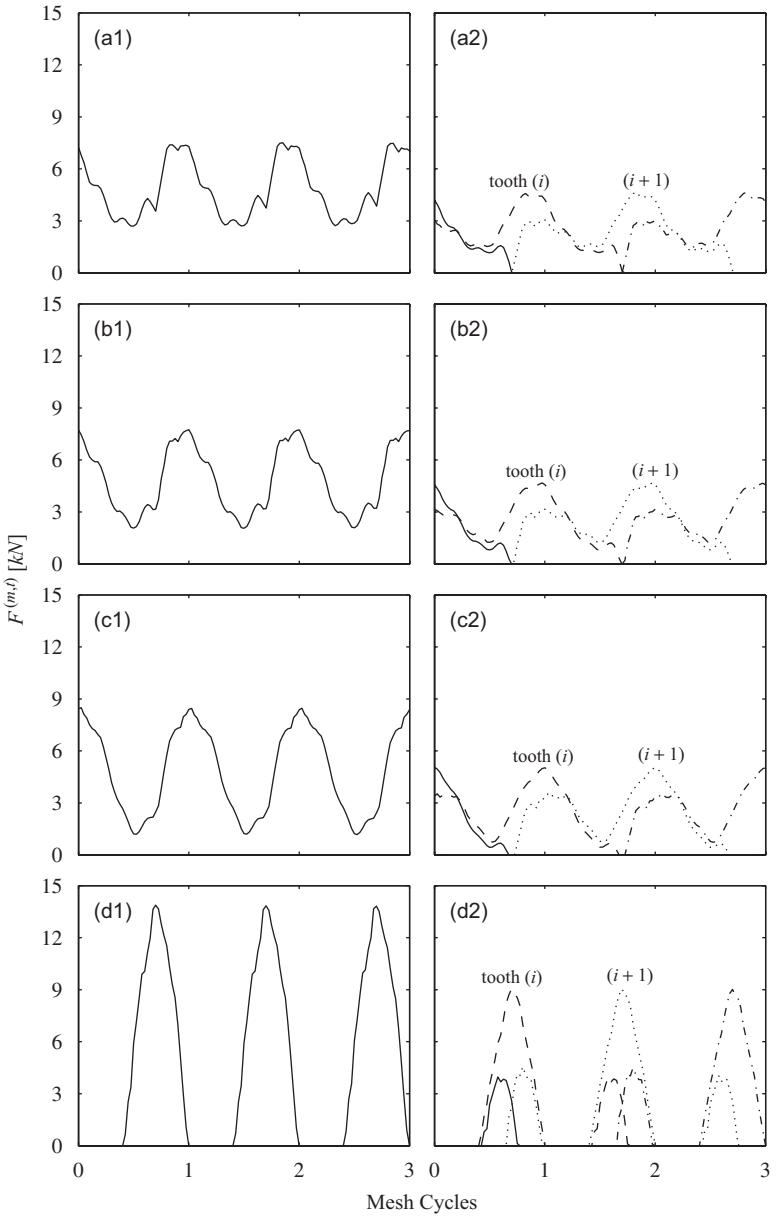

Fig. 11. Time histories of (a1–d1) $F^{(m)}$ and (a2–d2) $F^{(t)}$ of the example gear pair run at 2700 Hz on the upper branch after (a) 2 million cycles, (b) 10 million cycles, (c) 30 million cycles, and (d) 60 million cycles.

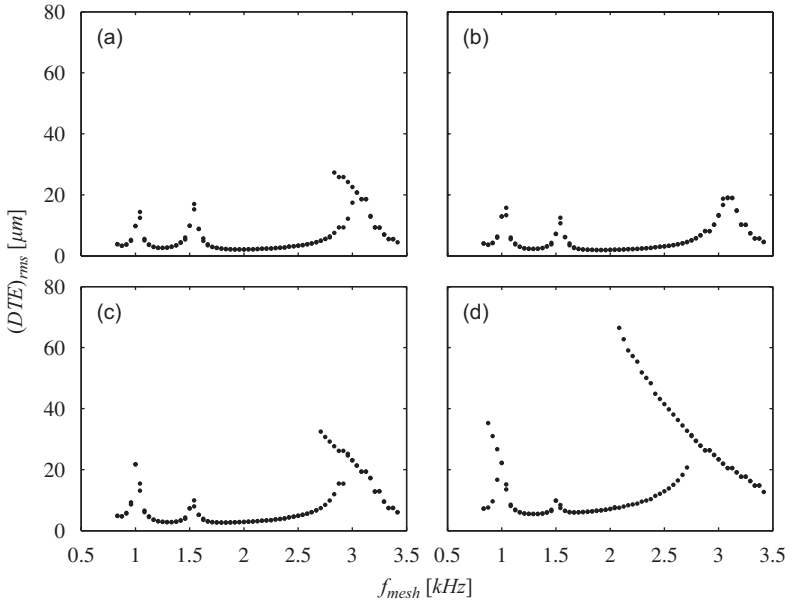

Fig. 12. Forced response of the example gear pair after operation at 2700 Hz on the upper branch for (a) 2 million cycles, (b) 10 million cycles, (c) 30 million cycles, and (d) 60 million cycles.

confirm this transformation of the nonlinear motions to linear ones and then again to nonlinear ones near the primary resonance peak.

The computational time required for a complete wear analysis by using the discrete dynamic model is reasonable. For instance a complete dynamic wear analysis at a given speed with 15 geometry updates and given damping values required about 10 min of CPU time on a 3.0 GHz PC. On the other end, the deformable-body model required nearly 25 times more time for the same analysis.

5.2. *Effect of dynamic response on wear*

The quasi-static wear profiles of the driving and driven gears are shown in Fig. 13(a) after different wear cycles to establish a baseline with no dynamic effects. Since spur gears with no lead modifications are used, only the wear profiles in the mid-plane of the gears after different wear cycles are shown here while the quasi-static analysis is indeed three-dimensional. It is evident from Fig. 13(a) that the maximum wear occurs in the dedendum region of the tooth while wear along the pitch line at a roll angle of 20.9° is nearly zero since there is theoretically no relative sliding to cause any wear. Driving and driven gears exhibit similar wear profiles since both gears are identical.

Dynamic wear profiles for the gear pair run at the same three operating conditions marked at Fig. 2 are illustrated in Fig. 13(b–d). First of all, dynamic wear profiles are clearly different from the static ones in both amplitudes and overall wear profile shapes. In Fig. 13(b), the wear profiles accumulated at 1540 Hz exhibit a waviness in the profile direction as a direct result of the oscillation of $F^{(m)}$ shown in Fig. 6(a). It was noted in Fig. 6(a) that the first harmonic component of the response is dominant since the operating speed is very near to the first super-harmonic resonance frequency, resulting in two well-defined fluctuations per gear mesh period. Since the example gear pair has a contact ratio of 1.8, indicating that each tooth remains loaded for 1.8 mesh cycles, it should then experience nearly (2)(1.8) = 3.6 cycles of loading at this particular mesh frequency. As a direct result of this, the wear profiles shown in Fig. 13(b) for both the pinion and gear exhibit a waviness that has formed by 3.6 periods.

In Fig. 13(c and d), the wear profiles of the gear pairs operated on the lower and upper branches of the steady-state response at 2700 Hz are illustrated. The wear profiles shown in Fig. 13(c) for the lower branch motions is quite similar to those of the lower frequencies, until the wear amounts become large enough to

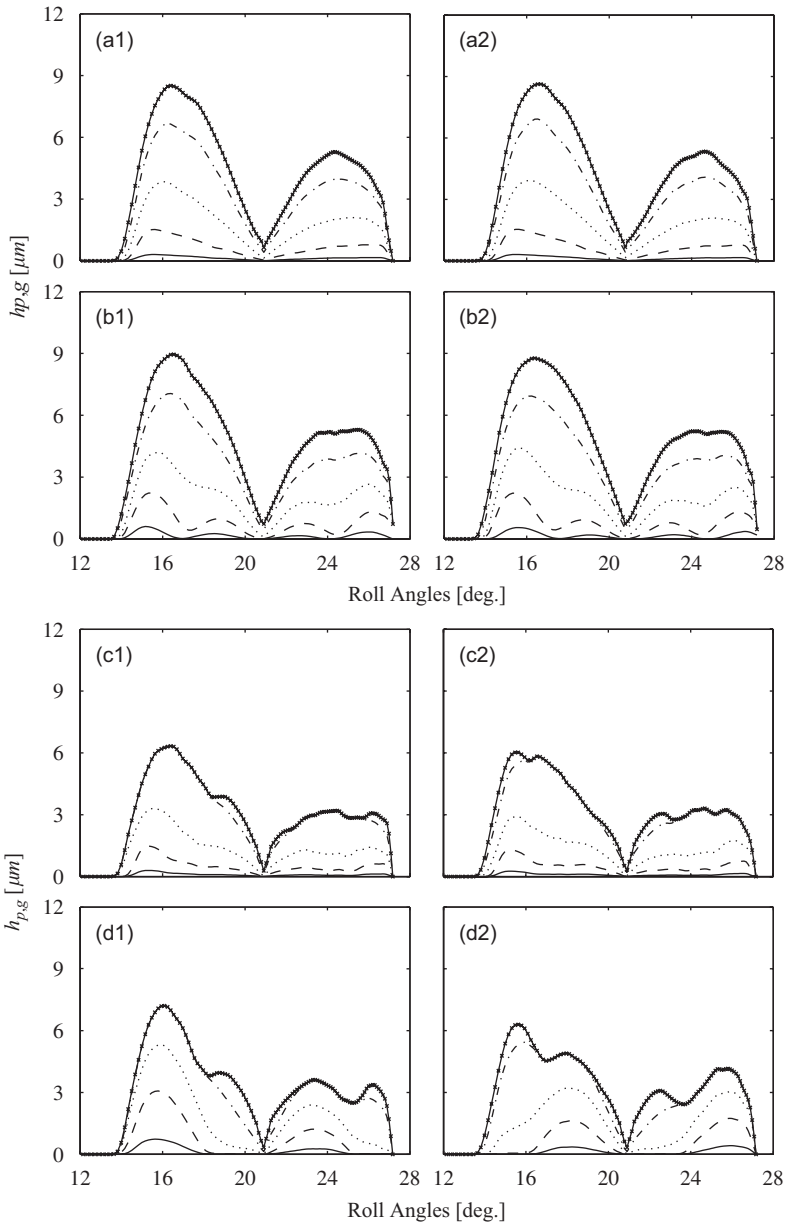

Fig. 13. Tooth wear profiles of (a1–d1) pinions and (a2–d2) gears operated at (a) quasi-static conditions, (b) 1540 Hz, (c) 2700 Hz on the lower branch, and (d) 2700 Hz on the upper branch. (—) 2 million cycles, (– –) 10 million cycles, (…) 30 million cycles, (–·–) 60 million cycles, and (–×–) 80 million cycles.

cause tooth separations. As shown in Fig. 9 earlier, this gear pair operated at this mesh frequency accumulates enough wear after 60 million cycles for separations to occur. In Fig. 9(d) after 60 million cycles, $F^{(m)}$ becomes zero within the roll angle ranges of 13.5–18.5° and 22.5–25.5° of the pinion. Therefore, the contact areas of tooth surfaces falling into these ranges do not accumulate additional wear after 60 million cycles. That is why the surface profiles at 60 and 80 million wear cycles are identical within these roll angle ranges. On the other hand, the upper branch motions of the gear pair having no wear exhibits tooth separations at 2700 Hz as shown in Fig. 6(d). As a result of this, the initial wear profiles shown in Fig. 13(d) have zero wear within the pinion roll angle ranges of 18–20.9° and 25–27°, corresponding to the mesh positions having tooth separation. With increased wear cycles, these bands of no wear are eliminated. For instance, wear is observed at every roll

angle after 30 million wear cycles. This is because the nonlinear behavior (tooth separations) is eliminated due to wear, as illustrated earlier in Fig. 11. Also in agreement with Fig. 11(d), tooth separations are reintroduced after 60 million wear cycles, resulting in a contact loss within the pinion roll angle ranges of 14–18° and 22.5–25°. Therefore, no additional wear is predicted within these ranges beyond 60 million wear cycles.

Wear behavior presented in Fig. 13 shows that the maximum wear amplitudes also change with speed, in addition to shapes of the wear profiles. In Fig. 13(b–d), the maximum wear depth value is slightly larger 1540 Hz, but somewhat lower at 2700 Hz, suggesting that there is not a simple trend here. The operating speed influences the dynamic mesh and tooth force amplitudes. For the two example mesh frequencies considered here, increasing speed results in increased mesh forces. This should increase the amount of wear. On the other hand, the wear coefficient, defined by Eq. (13), is dependent on $\lambda = h_{\min}/R_q$. At a given surface roughness value R_q, $h_{\min}$ increases with speed parameter $U = \eta_0 u/(E'R)$, and reduces with the load parameter $W = (L/b)/(E'R^2)$. Since $h_{\min}$ is proportional to $U^{0.68}$ and $W^{-0.073}$, the influence of speed on $h_{\min}$ is more pronounced. As a result, λ increases with speed, causing the wear coefficient k to reduce according to Eq. (13). In addition, the tooth separations near the resonance peaks also slow the accumulation of wear. These effects are all apparent in Figs. 7–13.

One potential concern with the model used is that it assumes constant backlash throughout the wear simulation. Even if actual backlash values might change with wear, these changes are at least an order of magnitude smaller than the nominal backlash values. Therefore, assumption of constant backlash should be reasonable. On the other hand, it is also assumed that the gear mesh damping value remains constant during the same wear process as well. This might be a more critical assumption that we intend to verify through controlled dynamic wear experiments.

6. Conclusions

Two different dynamic models and a surface wear model are combined here to study the interaction between surface wear and gear dynamic response. The proposed dynamic gear wear model includes the influence of worn surface profiles on dynamic forces and the motion transmission error as well as the influence of dynamic tooth forces on wear profiles. Simulation results indicate that there is a two-way interaction between wear and dynamic behavior in geared systems. Surface wear is shown to influence vibration amplitudes and the forced frequency response both quantitatively and qualitatively. In its initial stages, wear is shown to reduce the nonlinear forced response curves having softening-type jump discontinuities into linear ones by eliminating tooth separations. Such nonlinear behavior is predicted to reappear as wear amounts become more significant. Furthermore, the wear process influences each harmonic component of the response in different levels. When operated near a resonance peak, accumulating surface wear is shown to diminish this particular resonance peak. Likewise, both wear amplitudes and wear profile shapes are influenced significantly by the dynamic operating conditions. Smaller wear depths are predicted at higher operating speeds than those at lower speeds mainly because $h_{\min}$ is increased (and hence k is reduced) with speed.

Our ongoing work focuses on the effect of surface roughness variations on dynamic wear behavior and on an expansion of the dynamic wear model to helical gears and multi-mesh gear trains such as planetary gear sets. An experimental study is also in progress for validation of the dynamic wear model. We are pursuing this validation study in two ways. One focuses on the effect of dynamics on wear. For this, we have procured high-accuracy gear specimens having varying surface roughness levels. We are currently operating them under various levels of load and different types of lubricants (at various temperature levels) using FZG-type gear durability test machines and monitoring the resultant wear profiles through CMM inspections. Another activity focuses on the measurement of dynamic behavior of gears with wear using the same setup used in Refs. [4,7,8].

References

[1] K.J. Huang, T.S. Liu, Dynamic analysis of a spur gear by the dynamic stiffness method, *Journal of Sound and Vibration* 234 (2000) 311–329.

[2] S. Theodossiades, S. Natsiavas, Non-linear dynamics of gear–pair systems with periodic stiffness and backlash, *Journal of Sound and Vibration* 229 (2000) 287–310.

[3] R. Maliha, U. Dogruer, H.N. Ozguven, Nonlinear dynamic modeling of gear-shaft-disk-bearing systems using finite elements and describing functions, *Journal of Mechanical Design* 126 (2004) 534–541.
[4] G.W. Blankenship, A. Kahraman, Steady state forced response of a mechanical oscillator with combined parametric excitation and clearance type nonlinearity, *Journal of Sound and Vibration* 185 (1995) 743–765.
[5] R.G. Munro, Dynamic Behaviour of Spur Gears, PhD Dissertation, Cambridge University, 1962.
[6] K. Umezawa, T. Sata, J. Ishikawa, Simulation of rotational vibration of spur gears, *Bulletin of JSME* 38 (1984) 102–109.
[7] A. Kahraman, G.W. Blankenship, Interactions between commensurate parametric and forcing excitations in a system with clearance, *Journal of Sound and Vibration* 194 (1996) 317–336.
[8] A. Kahraman, G.W. Blankenship, Experiments on nonlinear dynamic behavior of an oscillator with clearance and time-varying parameters, *Journal of Applied Mechanics* 64 (1997) 217–226.
[9] Y. Chen, M. Matubara, Effect of automatic transmission fluid on pitting fatigue strength of carborized gears, *JSME International Conference on Motion and Power Transmission*, Fukuoka, Japan, 2001, pp. 151–156.
[10] J.F. Archard, Contact of rubbing flat surfaces, *Journal of Applied Physics* 24 (1953) 981–988.
[11] A. Flodin, S. Andersson, Simulation of mild wear in spur gears, *Wear* 207 (1997) 16–23.
[12] P. Bajpai, A. Kahraman, N.E. Anderson, A surface wear model for parallel axis gear pairs, *Journal of Tribology* 126 (2004) 597–604.
[13] C. Yuksel, A. Kahraman, Dynamic tooth loads of planetary gear sets having tooth profile wear, *Mechanisms and Machine Theory* 39 (2004) 695–715.
[14] V.K. Tamminana, A. Kahraman, S. Vijayakar, An investigation of the relationship between the dynamic transmission error and dynamic factors of a spur gear pair, *Journal of Mechanical Design* 129 (2007) 75–84.
[15] EXTPAIR-2D User's Manual, Advanced Numerical Solutions, Inc., 2004.
[16] T.F. Conry, A. Seireg, A mathematical programming technique for the evaluation of load distribution and optimal modifications for gear systems, *ASME Journal of Engineering for Industry, Series B* 95 (1973) 1115–1122.
[17] M. Priest, C.M. Taylor, Automobile engine tribology—approaching the surface, *Wear* 241 (2000) 193–203.
[18] D. Dowson, Modelling of elasto-hydrodynamic lubrication of real solids by real lubricants, *Meccanica* 33 (1998) 47–58.